Liquid Crystals
Publication details, including instructions for authors and subscription information:
http://www.informaworld.com/smpp/title~content=t713926090

Second-harmonic generation in a novel crosslinked pyroelectric liquid crystal polymer (PLCP)

D. S. Hermann; P. Rudquist; S. T. Lagerwall; L. Komitov; B. Stebler; M. Lindgren; M. Trollsas; F. Sahlen; A. Hult; U. W. Gedde; C. Orrenius; T. Norin

Online publication date: 06 August 2010

To cite this Article Hermann, D. S. , Rudquist, P. , Lagerwall, S. T. , Komitov, L. , Stebler, B. , Lindgren, M. , Trollsas, M. , Sahlen, F. , Hult, A. , Gedde, U. W. , Orrenius, C. and Norin, T.(1998) 'Second-harmonic generation in a novel crosslinked pyroelectric liquid crystal polymer (PLCP)', Liquid Crystals, 24: 2, 295 — 310
To link to this Article: DOI: 10.1080/026782998207479
URL: http://dx.doi.org/10.1080/026782998207479

LIQUID CRYSTALS, 1998, VOL. 24, NO. 2, 295–310

Second-harmonic generation in a novel crosslinked pyroelectric liquid crystal polymer (PLCP)

by D. S. HERMANN*, P. RUDQUIST, S. T. LAGERWALL, L. KOMITOV, B. STEBLER

Department of Microelectronics and Nanoscience, Chalmers University of Technology, S-412 96 Göteborg, Sweden

M. LINDGREN

Department of Physics and Measurement Technology, Linköping University, S-581 83 Linköping, Sweden; Department of Laser Systems, Defence Research Establishment, Box 1165, S-581 11 Linköping, Sweden

M. TROLLSÅS, F. SAHLÉN, A. HULT, U. W. GEDDE

Department of Polymer Technology, Royal Institute of Technology, S-100 44 Stockholm, Sweden

C. ORRENIUS and T. NORIN

Department of Chemistry, Organic Chemistry, Royal Institute of Technology, S-100 44 Stockholm, Sweden

(*Received 1 April 1997; accepted 15 September 1997*)

We report second-harmonic generation in samples with a pyroelectric liquid crystal polymer (PLCP) prepared from the ferroelectric liquid crystalline acrylate monomer 4-[(*R*)-(-)-2-(10-acryloyloxydecyl)oxy]-3-nitrophenyl 4-[4-(11-acryloyloxyundecyloxy)phenyl]-benzoate (**A2c**) by *in situ* photopolymerization. The relation between SHG efficiency, spontaneous polarization and amount of chiral substance in this and previously synthesized PLCP materials is discussed. Electro-optical properties of the monomeric and crosslinked **A2c** are investigated. In the crosslinked state, the molecular mobility is found to be very low, supporting the fact that the degree of polar order in the polymer is high. In contrast to the case of a poled electret NLO material, the polarization of this material is *not* 'frozen-in', but an intrinsic thermodynamic property.

1. Introduction

The ultra-fast, non-resonant optical non-linearities of molecular electronic origin in organic and polymeric materials have attracted great research interest during the last decade. These materials offer the possibility of combining properties such as high intrinsic molecular hyperpolarizability, synthetic flexibility for optimization of non-linear optical effects and in addition good thermal and mechanical stability; also they are relatively cheap and easy to process [1]. Dipolar order is a requirement for second-order non-linear optical processes. A common problem with organic and polymeric materials, however, is their low degree of polar order. The reason is that it is not intrinsic: the material has to be polarized to some degree by a strong external field. This state has been frozen in. Electrically speaking, the material is in a glassy state, analogous to a magnetic spin-glass where the magnetically aligned spin moments have been frozen in.

Liquid crystals are generally orientationally ordered organic materials, but without dipolar order. The local anisotropy axis, the director, has quadrupolar symmetry in the sense that the lowest multipole moment that does not vanish along the director is the quadrupole moment. The local symmetry of the director is D_∞ (Schönfliess). Ferroelectric liquid crystals [2, 3] (FLCs) are chiral tilted smectics which are quite special because their symmetry allows a local dipolar order perpendicular to the tilt plane [2]. This means that at right angles to the director we have a polar axis, of local symmetry C_2.

*Author for correspondence.

0267–8292/98 $12·00

Under certain circumstances (surface stabilization) this can be transferred to the whole medium, which then acquires a macroscopic polar symmetry [3]. In order for this polar axis to stay in a fixed direction, an external electric field might be applied. Such a field is not necessary if the surface stabilization is perfect. Mostly this is not the case. Our aim is to develop a material with a high degree of polar order (high $\chi^{(2)}$) that is also thermodynamically stable, both in magnitude and direction, and as independent as possible of electric field and temperature, and even of surfaces.

The first measurements of second-harmonic generation in FLCs were carried out in 1981 by Vtyurin *et al.* [4] using DOBAMBC. Phase-matched SHG in DOBAMBC was reported in 1985 by Shtykov *et al.* [5]. In these as well as in the experiments to be cited in the following text, a d.c. electric field of the order of $0{\cdot}1\ \mathrm{V}\,\mu\mathrm{m}^{-1}$ was applied across the sample to line up the director homogeneously. The synthesis by Walba *et al.* [6] of compound **I** (figure 1) was carried out in 1990 with the specific purpose of increasing the second-order optical non-linearity, measured to be $d_{22} = (0{\cdot}6 \pm 0{\cdot}3)\ \mathrm{pm\ V}^{-1}$ [7]. Since then, a great effort has gone into the synthesis and characterization of new FLC materials intended for NLO applications. In 1993, Schmitt *et al.* [8] synthesized 4-ring compounds such as **II** (figure 1) with an electron donor amino group in the *para*-position to the electron acceptor nitro group, thus creating a strong NLO chromophore perpendicular to the molecular long axis. The effective second-order non-linear optical coefficient was reported to be $d_{22} \sim 5\ \mathrm{pm\ V}^{-1}$ at phase-matching, which is comparable to that for inorganic non-linear optical materials. Several other studies of SHG in ferroelectric liquid crystals [9–15] and ferroelectric liquid crystal side group polymers [16, 17] have been carried out. Recently, SHG induced by the electroclinic effect in the SmA* phase was also reported [18].

The problem with the ferroelectric liquid crystalline state, however, is that the polar order is thermally limited to the SmC* phase (or any other chiral tilted smectic phase), and it has poor mechanical properties. A way to overcome these problems is a stabilization by photoinitiated crosslinking, creating a thermally and mechanically stable polymeric network which is no longer switchable, and therefore not ferroelectric but pyroelectric. In 1995 the acrylate compounds **A1** and **A2** (figure 1) were synthesized, and stable, pyroelectric liquid crystal polymer (PLCP) networks from mixtures of these were made which showed second-harmonic generation [19, 20]. **A1** is the chiral monomer, and it is monofunctional. **A2** is non-chiral, but bifunctional, in order to allow crosslinking. Later, the compounds **A1b** and **A2b** were synthesized, and mixtures of different combinations of these and of **A1** and **A2** were examined with respect to their spontaneous polarization [21]. The aim was to increase the concentration of NLO chromophores, in order to increase the non-linear optical response, by adding lateral nitro groups to the non-chiral bifunctional monomer. However, the spontaneous polarization increased only when the concentration of chiral monomers was increased in the mixture. In 1996 a single monomer, **A2c**, was therefore synthesized which combines chirality and bifunctionality in one compound [22]. This compound shows a large spontaneous polarization (160–$170\ \mathrm{nC\,cm}^{-2}$) in the SmC* phase at room temperature.

2. Experimental

Shear cells of conventional sandwich type were filled with the monomer **A2c**. Five samples with **A2c** were prepared, which in the following will be denoted **A**, **B**, **C**, **D** and **E**. The spacer thickness was $2\ \mu\mathrm{m}$ for samples **A–C** and **E**, and $4\ \mu\mathrm{m}$ for sample **D**. The spacers were prepared by evaporating SiO directly onto the glass plates.

In samples **A-C**, the monomer was mixed with the photoinitiator Lucirin TPO in the proportion 250 : 1 (see figure 2). In samples **D** and **E** the pure monomer was used. Good planar alignment in the bookshelf geometry was obtained by shear with the simultaneous application of an a.c. electric field. After initial heating to 40°C and slow cooling into the SmC* phase at room temperature, a clear, ferroelectric switching was obtained with a tilt angle of more than 30°. At 25°C the ferroelectric liquid crystalline acrylate monomer in samples **A–C** was crosslinked by UV-photopolymerization while applying an electric d.c. field, selecting a definite direction of the optic axis, thus creating a thermally stable, optically anisotropic poled polymer network. The resulting locked-in SmC* tilt angle of the polymer network turned out to vary between the samples which were designated **A**, **B** and **C** in order of decreasing tilt (see the table).

Measurements of second-harmonic generation were carried out on samples **A**, **B** and **D** in two different set-ups with pulsed Nd : YAG lasers. The measurements on sample **A** were carried out with a Spectron laser operating at 1064 nm wavelength with a pulse width of 10 ns at a repetition rate of 10 Hz. The measurements on samples **B** and **D** were carried out with a Continuum Sunlite OPO laser system with a pulse width of 7–8 ns at a repetition rate of 10 Hz, which in the present experiment was set to operate at 1100 nm wavelength. In both cases, one or several visible-cut filters were placed in front of the sample allowing only fundamental light to reach the sample, and an IR-cut filter was placed behind the sample, eliminating any remaining fundamental light after the sample.

In the Sunlite OPO set-up, one or several narrow band-pass filters were also placed in front of the detector

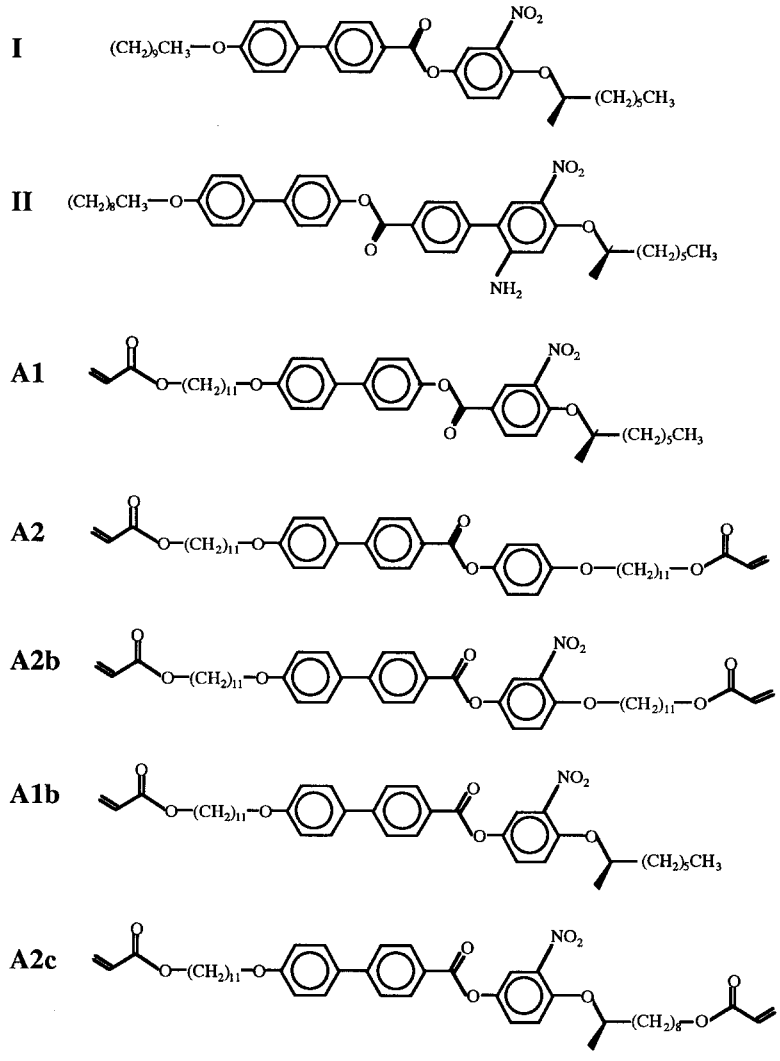

Figure 1. The chemical structures of the compounds **I** [6], **II** [8], and of the mono- and bi-functional acrylate monomers **A1**, **A2**, **A1b**, **A2b** and **A2c**.

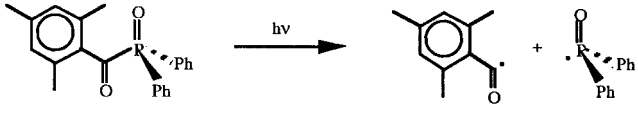

Figure 2. The photoinitiator Lucirin TPO, and the reaction on UV-illumination. Both products of the reaction are active in the subsequent polymerization process.

Table. The locked-in tilt angle of the polymerized samples.

Sample	Tilt angle/°
A	33
B	24
C	20

($\Delta\lambda = 5$–10 nm) to ensure that only the second harmonic light was detected. The signal from the photomultiplier could thus be attributed to the visible, second-harmonic light generated in the sample. The intensity of the fundamental light was simultaneously measured by a second photomultiplier or photodiode. With a polarizer for infrared light before the sample and an analyser for visible light after the sample, the polarization combinations p-p and p-s were selected, with p denoting the polarization direction in the plane of incidence and s denoting the polarization direction orthogonal to the plane of incidence. In the SHG measurements no electric field was applied to the crosslinked samples; to sample **D**, a d.c. bias field (100 V across 4 μm) was applied.

The electro-optic measurements were carried out on samples **A**–**C** and **E** with a standard electro-optic set-up

based on a polarizing microscope with an angular turntable. The sample was turned so that its optic axis made an angle of 22·5° with the polarizer, to obtain linear detection. The optical transmission through crossed polarizers was monitored by a photodiode connected to an oscilloscope. An applied a.c. electric field of triangular wave shape was applied to the samples.

3. Physical properties of the monomer A2c

The monomer **A2c** was found to have two liquid crystalline phases between the solid (crystal) and the isotropic liquid states. The low temperature phase is the SmC* phase, where a clear, ferroelectric switching could be observed. The high temperature phase, however, has not yet been identified clearly. The transition temperature between the SmC* phase and the high temperature phase was about 33°C on heating, and about 1° lower on cooling.

The low temperature phase (SmC*) and the high temperature phase are both highly twisted phases. In the case of the SmC* phase the pitch is about 0·4 μm [22]. In the case of the high temperature phase, when no electric field is applied, a characteristic blue texture is observed using the polarizing microscope, indicating a helical structure of the liquid crystal with the helix axis normal to the cell glass plates (see figure 3). Upon lowering the temperature into the SmC* phase, a planar texture with several, small domains appears spontaneously.

At low electric field strengths in the SmC* phase, below a critical field, the SmC* helix is only partially unwound. This deformed helix switching gives a linear deflection of the optic axis with the electric field. The critical field for unwinding the SmC* helix completely is about 3 V μm^{-1}. At higher electric field strengths the current and optical responses typical of a ferroelectric liquid crystal are observed.

Applying an electric field in the high temperature phase, at a certain electric field strength the blue texture changes into a parallel aligned texture. The transition between the two textures is quite sharp. In slightly wedge-shaped samples it is possible to observe a clear border between the two textures at a certain applied voltage, due to the changing electric field strength caused by the varying distance between the electrodes. This border is readily moved back and forth when the voltage is slightly varied. In the planar texture the liquid crystal switches: i.e. the electric field induces an in-plane deflection of the optic axis of the sample.

A measurement on sample **E** of the field-induced deflection of the optic axis in the two phases on the application of a constant electric field of 35 V μm^{-1} is shown in figure 4 as a function of temperature. In the SmC* phase, the deflection is of the usual molecular tilt angle of the mesogens with respect to the smectic layer normal, which is found to decrease with increasing temperature. In the high temperature phase, the field-induced deflection of the optic axis, which lies in the plane of the cell, was inferred from the measured angular difference between the two extreme orientations of the optic axis at positive and negative applied voltage. The angle of this deflection is found to be about 15° at 35 V μm^{-1}, and virtually independent of temperature.

The experimental findings are inconsistent with a SmC*–SmA* phase transition, in particular the existence of a helical axis at zero field in the high temperature phase. Possible alternatives as to the nature of the high temperature phase of **A2c** are a tightly twisted cholesteric phase or some TGB phase, like TGBC*. However, the temperature range of about 5–6 degrees is relatively broad for a TGB phase. The absence of hysteresis in the electric field strength in the transition between the standing helix and the in-plane optic axis textures, as well as the small thickness of the sample cells (2–4 μm), make a TGB phase unlikely. The correct phase assignment is thus more likely to be cholesteric than TGB. With this interpretation, the observed field-induced deflection of the optic axis is nothing but the flexoelectro-optic effect in a short pitch cholesteric liquid crystal in the uniform lying helix (ULH) texture [23, 24]. The field-induced helix deformation in the cholesteric phase would then give a linear deflection of the optic axis as a function of the applied electric field, but would be independent of the temperature.

The nature of the cholesteric or cholesteric-like phase of **A2c** is currently being investigated in more detail.

4. Electro-optic investigations of the polymer network

If the mesogenic units in the polymer network are not completely locked-in by the crosslinking, they will still have the possibility of reorienting slightly. It is then possible to induce a slight deviation from the locked-in tilt angle through the coupling between the applied electric field and the spontaneous polarization of the material, i.e. through the electroclinic effect [25]. This effect was found in all three polymerized samples, and measurements of the induced tilt angle as function of the applied electric field are shown in figures 5 (*a*) and 5 (*b*) for sample **B** and sample **C**, respectively. The frequency dependence of the induced tilt angle was measured for samples **A**, **B** and **C**, as shown in figures 6 (*a*)–(*c*).

The induced tilt angle varies linearly with the applied electric field, as expected for the electroclinic effect, but the magnitude of the induced tilt angle is of the order of 0·1° for samples **B** and **C**, and about 0·4° for sample **A**. These tilt angle values are very low, and they correspond to an angular deviation of the director of 0·4%,

0·5% and 1·2%, respectively, with respect to the locked-in tilt angles given in the table.

The induced tilt angle does *not* follow a simple Debye relaxation with a single relaxation time and a cut-off frequency. The behaviour of the induced tilt angle expected from the simple Debye relaxation is shown by the solid curve in figure 6(*a*), calculated for a cut-off frequency of 1 kHz. At low frequencies, the induced tilt angle would be independent of the frequency; at higher frequencies, the induced tilt angle would start to decrease. The decrease would depict a straight line with a constant, negative slope, when plotted in a linear logarithmic diagram. The cut-off frequency is defined by the constant, low frequency value of the induced tilt angle divided by $2^{1/2}$. The induced tilt angle which was measured for the polymer networks, however, is found to decay very quickly with frequency, depicting a frequency-dependent negative slope in the linear logarithmic diagram. In no frequency region is the value of the induced tilt angle found to be frequency-independent. The cut-off frequency is thus zero. This indicates that the mesogenic units are strongly hindered in their reorientation.

The frequency measurement was carried out particularly carefully for sample **C** at room temperature, and at very high frequencies an interesting phenomenon occurred. The induced tilt angle decreased for frequencies up to about 100 kHz. At higher frequencies the amplitude of the optical response started increasing again. At the same time the temperature of the sample, which was continuously measured during the entire measurement, started increasing slightly. A slight shift in the relative phase between the applied electric field and the optical response could also be observed. Below 100 kHz the temperature of the sample was 25–26°C; at 200 kHz the sample temperature was 27·7°C. At a frequency of 1 MHz the temperature of the sample increased very quickly, and was measured to be 37·7°C. At the same time the relative phase between the optical response and the applied electric field had shifted to about a quarter of a period. The polymer network thus has a resonance frequency in the MHz range, causing a strong spontaneous heating of the sample.

On the low frequency side, a marked drop in the induced tilt angle was observed below 40 Hz. A saturation of the optical response was observed in this frequency region, suggesting the screening of the applied electric field by free charges.

5. Chiral strength and spontaneous polarization

The spontaneous polarization for the monomers **A1**, **A2**, **A1b** and **A2b** mixed in different proportions was reported in [21], and it was concluded that only the lateral dipoles which are close to a chiral centre give a contribution to the spontaneous polarization. Hence, attaching nitro groups to the achiral bifunctional mesogenic acrylate monomer (i.e. turning **A2** into **A2b**) does *not* make the value of the spontaneous polarization increase. Moreover, the dependence of the spontaneous polarization on the molar percentage of chiral mesogenic monomers was found to be non-linear. These points are made evident in figure 7, where the data from [21] have been replotted for the different mixtures as functions of the molar percentage of chiral monomers, at the reduced temperature $\tau \equiv T/T_C = 0{\cdot}96$. Included in figure 7 is also the value of the spontaneous polarization of **A2c** at $\tau = 0{\cdot}96$, obtained from P_S data in [22].

The spontaneous polarization is thus highly dependent upon the molar concentration of chiral centres in a SmC* mixture. Since second-harmonic generation occurs only in non-centrosymmetric media, the second-order optical non-linearity of a SmC* or SmC* based material must also depend on the concentration (i.e. mole fraction) of chiral solute, which we might loosely call '*chiral strength*'. A correlation between the temperature dependence of the spontaneous polarization and that of the NLO d-coefficients has been reported several times before in the literature for ferroelectric liquid crystals [7, 8, 15].

There are mainly two contributions to the non-linear dependence of the spontaneous polarization on the molar percentage of chiral units. One is the difference in size (i.e. volume) of the two different molecules. The other is the dependence of the polar order (i.e. the bias in the rotational distribution of lateral dipoles around the molecular long axis) on the chiral strength.

The spontaneous polarization, under the assumption of perfect nematic order ($S = 1$), can be expressed as [15]

$$P_S = N\langle\mu\rangle \tag{1}$$

where N is the number density of lateral dipole moments and $\langle\mu\rangle$ is the average value of the lateral dipole moment with respect to the degree of polar order. In a mixture consisting of two differently sized molecular species A and B, N is the number density of chiral species A. The number density is in turn the number X_A of chiral species A per unit of volume of the mixture, $N = X_A/V_{tot}$ where $V_{tot} = V_A + V_B$ under the assumption of an ideal mixture, which is equivalent to the volume fraction v_A of the chiral species divided by the (microscopic) volume b_A of a molecule of the chiral species (see the Appendix). In other words, N in equation (1) is directly proportional to the volume fraction v_A.

The dependence of the volume fraction v_A on the mole fraction X_A of chiral species A in the mixture is given

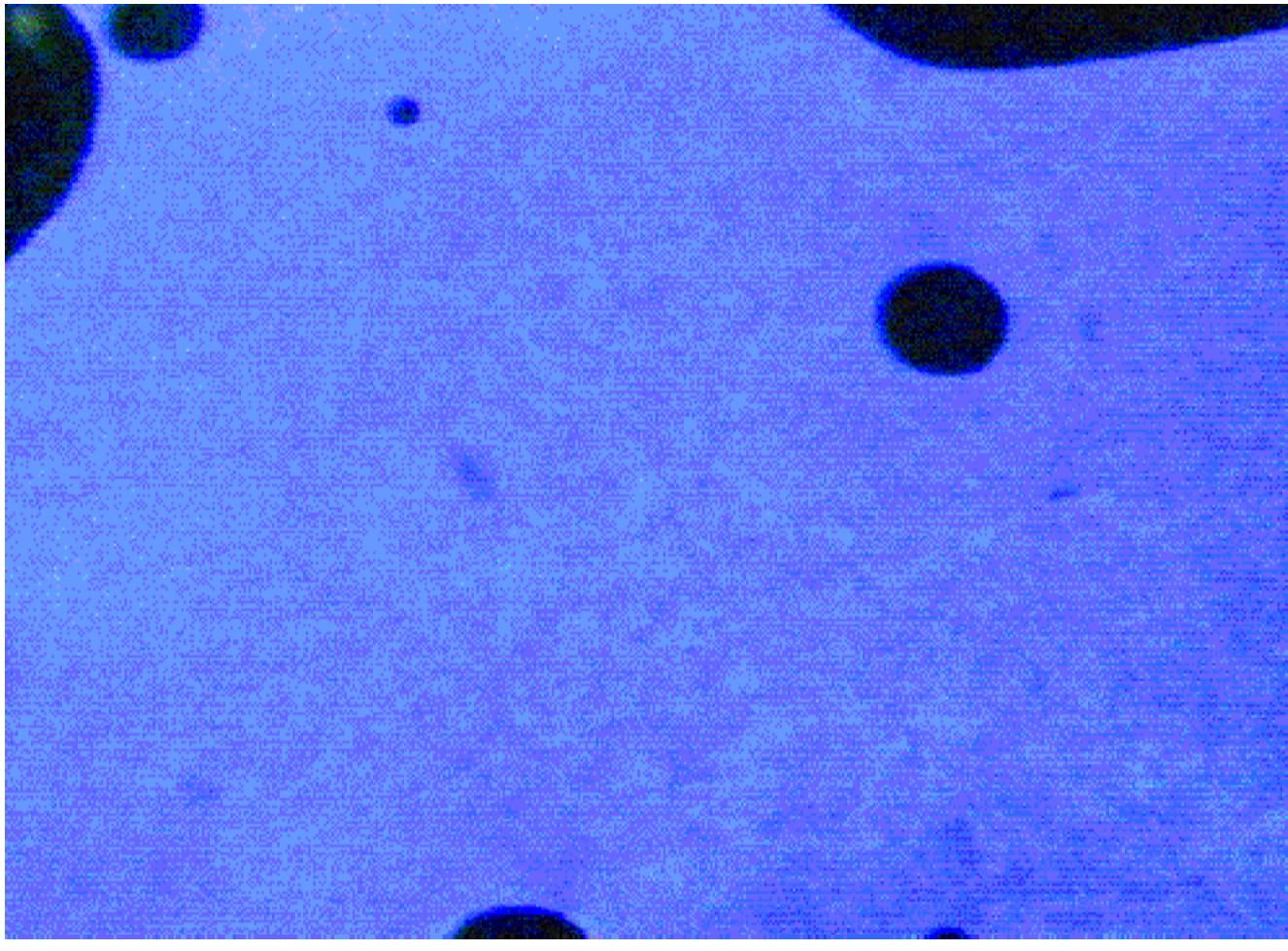

Figure 3. The blue texture of high temperature phase of the monomer **A2c**, implying a standing helical structure of the liquid crystal.

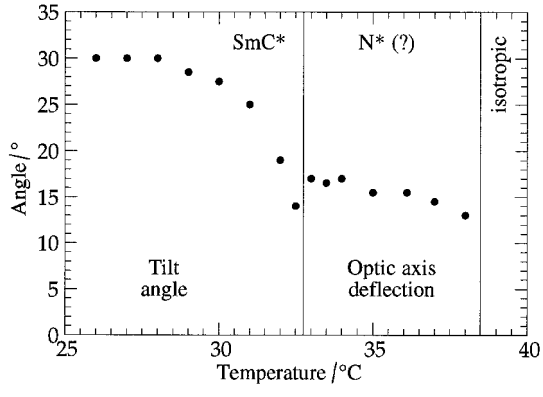

Figure 4. The tilt angle in the SmC* phase and the field-induced optic axis deflection in the high temperature phase as a function of temperature of the monomer **A2c**, under an applied electric field of 35 V μm^{-1}.

by (see the Appendix for a derivation)

$$v_A = \frac{\eta x_A}{1 + (\eta - 1) x_A} \qquad (2)$$

where $\eta \equiv b_A/b_B$ denotes the relation between the (microscopic) volumes $b_{A,B}$ of molecules A and B, respectively. Equation (2) is a non-linear function of the mole fraction, which directly gives a non-linear behaviour of the spontaneous polarization on the mole fraction x_A. It may be noted that if the molecules of the two species have the same volume ($\eta = 1$), then the volume fraction equals the mole fraction exactly. If species A is bigger than species B ($\eta > 1$), the curvature of equation (2) is negative ($d^2 v_A/dx_A^2 < 0$), and *vice versa*. The positive curvature described by the data in figure 7 is consistent with the monofunctional monomer being smaller than the bifunctional monomer.

In the limit of pure achiral component B, the medium becomes centrosymmetric. It follows that there can be no net lateral dipole moment in this case, implying $\langle \mu \rangle = 0$ when $x_A = 0$. From this it follows that the average value of the lateral dipole moment must depend on x_A.

The average lateral dipole moment in the SmC* phase is in general given by a microscopic model for the

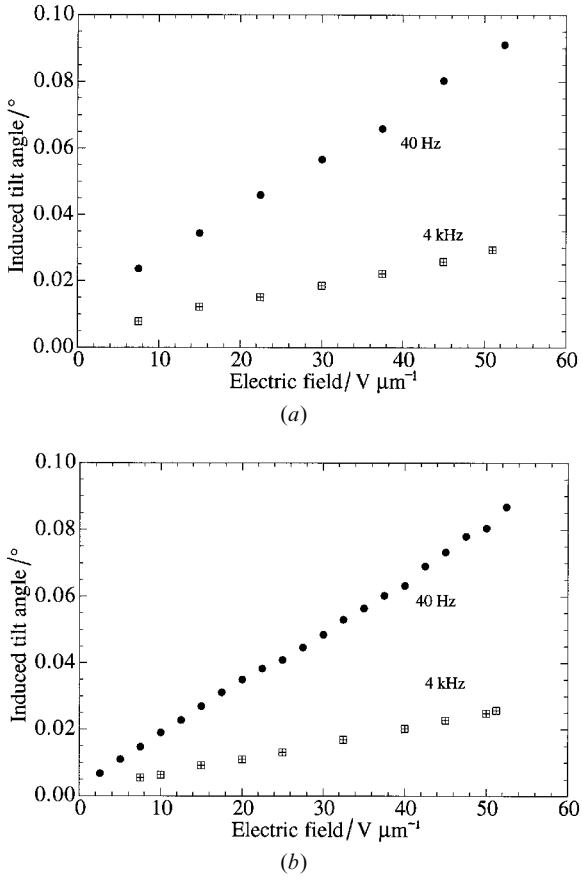

Figure 5. The field-induced deviation of the mesogenic units from the locked-in tilt angle of the polymer network of **A2c**, as function of applied electric a.c. field at 40 Hz and 4 kHz, respectively. (*a*) Sample **B**; (*b*) sample **C**.

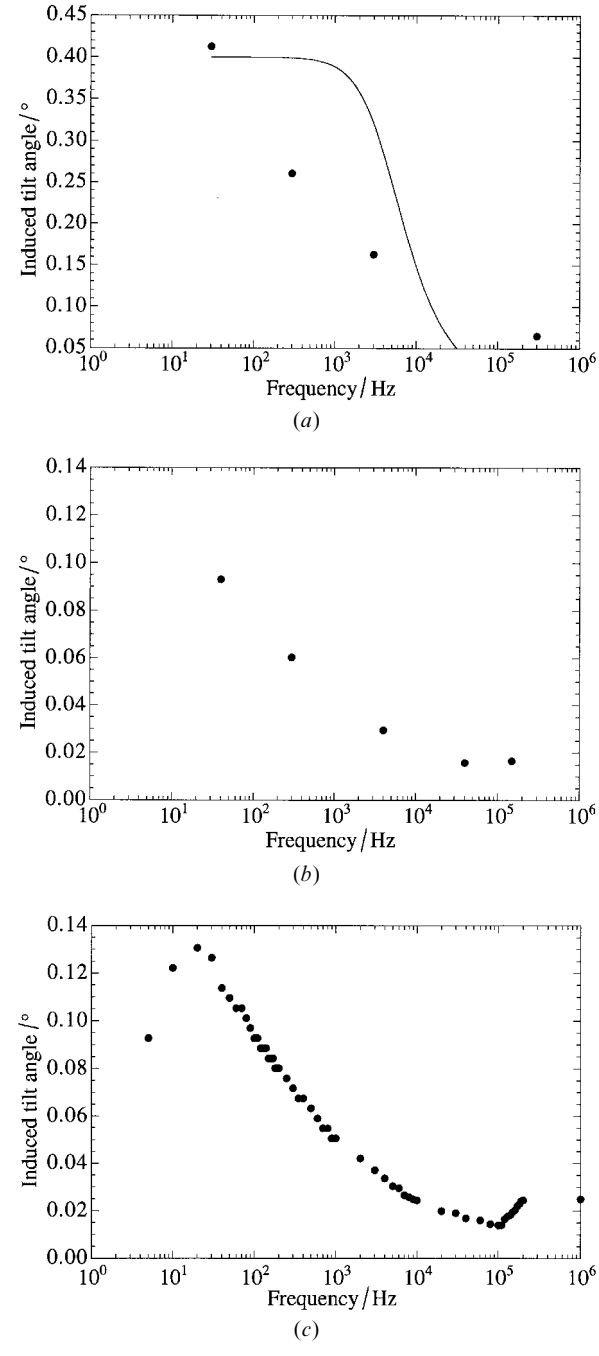

Figure 6. The field-induced deviation of the mesogenic units from the locked-in tilt angle of the polymer network of **A2c**, as function of the frequency of the applied electric a.c. field, at 50 V μm^{-1}. (*a*) Sample **A**; (*b*) sample **B**; (*c*) sample **C**.

rotation of the molecules around their long axes [26, 27]:

$$\langle \mu \rangle = \mu_{\perp} \langle \cos \psi \rangle \tag{3}$$

where ψ is the angle of rotation around the molecular long axis and $\mu_{\perp}$ is the microscopic lateral dipole moment of one molecule. When $\psi = 0$, the molecular dipole points in the same direction as the C_2 axis. $\langle \cos \psi \rangle$ is the order parameter of the lateral dipoles, and is given by the Boltzmann average

$$\langle \cos \psi \rangle = \frac{\int_0^{2\pi} \cos \psi \exp[-U(\psi)/kT] \, d\psi}{\int_0^{2\pi} \exp[-U(\psi)/kT] \, d\psi} \tag{4}$$

where the potential U is given by

$$U(\psi) = -a_1 \theta \cos \psi - a_2 \theta^2 \cos 2\psi. \tag{5}$$

The first term, being linear in the tilt, describes the dipolar order and is therefore chiral. The second term, being quadratic in the tilt, describes the quadrupolar order and is therefore achiral. The potential has minima at $\psi = 0$ and $\psi = \pm\pi$, where the minimum at $\psi = 0$ is deeper due to the chiral term. It thus biases the rotational distribution of the molecular dipoles around the molecular long axis, in the direction of the C_2 axis.

If x_A is the mole fraction of chiral solute, then the chiral term in equation (5) will have less influence on

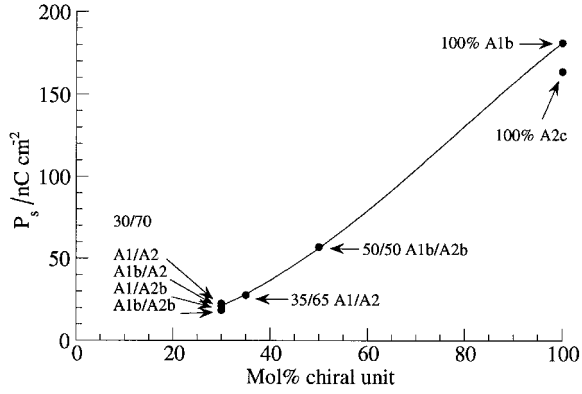

Figure 7. The spontaneous polarization of mixtures of some of the acrylate monomers shown in figure 1, as a function of the content of chiral monomers at the reduced temperature $\tau \equiv T/T_C = 0{\cdot}96$. The solid line is a curve fit, as explained in the text; **A2c** was not included in the curve fit.

the rotational distribution of the lateral dipole. This may be taken into account by multiplying the chiral term by x_A, so that the following potential is obtained for a dilute system:

$$U(\psi, x_A) = -a_1 x_A \theta \cos\psi - a_2 \theta^2 \cos 2\psi \qquad (6)$$

where $x_A \in [0, 1]$. Inserting equation (6) into (4) gives

$$\langle \cos\psi \rangle = a_1 x_A \theta \frac{2kT + a_2\theta^2}{4(kT)^2 + (a_1\theta)^2 x_A^2 + (a_2\theta^2)^2}. \qquad (7)$$

Rewriting equation (7) in terms of two dimensionless parameters κ and γ, making explicit the dependence on the mole fraction x_A, the dependence on x_A of the average dipole moment $\langle \mu \rangle$ is obtained as

$$\langle \mu \rangle = \mu_\perp \frac{\kappa x_A}{1 + \gamma x_A^2} \qquad (8)$$

where

$$\kappa = \frac{\dfrac{2kT}{a_2\theta} + \theta}{\dfrac{4k^2T^2}{a_1 a_2 \theta^2} + \dfrac{a_2}{a_1}\theta^2} \quad \text{and} \quad \gamma = \frac{a_1}{\dfrac{4k^2T^2}{a_1\theta^2} + \dfrac{a_2^2}{a_1}\theta^2}. \qquad (9)$$

Inserting equations (2) and (8) into equation (1) the following relation is obtained for the spontaneous polarization as a function of mole fraction x_A of chiral species A:

$$P_S = N\langle \mu \rangle = \frac{\mu_\perp \kappa}{b_A} \eta \frac{x_A^2}{[1 + \gamma x_A^2][1 + (\eta - 1)x_A]}. \qquad (10)$$

Equation (10) was fitted to the spontaneous polarization data, with $\mu_\perp \kappa / b_A$ and γ being the fitting parameters, for different fixed values of η in the range 0·6 to 1·2. The best fit was obtained for the value $\eta = 0{\cdot}78$, giving the values $\mu_\perp \kappa / b_A = (295 \pm 11)\,\mathrm{nC\,cm^{-2}}$ and $\gamma = (6{\cdot}26 \pm 0{\cdot}66) \times 10^{-3}$, and is shown as the solid line in figure 7. The result $\eta = 0{\cdot}78$ means that the volume of an individual monofunctional chiral monomer is about 80% of that of the bifunctional achiral monomer. This is a reasonable result considering the structural formulae of the monomers **A1** and **A1b** with respect to **A2** and **A2b**.

6. Chiral strength and the second-order NLO susceptibility

The second-order non-linear optical coefficient $\chi^{(2)}$ is given by [1]

$$\chi^{(2)} = NF\langle \beta \rangle \qquad (11)$$

where $\langle \beta \rangle$ is the average value of the molecular hyperpolarizability with respect to the degree of order, $F = f_{2\omega} f_\omega f_\omega$ is the product of the Lorentz local field factors given by

$$f_\omega = \frac{(n_\omega)^2 + 2}{3}; \qquad f_{2\omega} = \frac{(n_{2\omega})^2 + 2}{3} \qquad (12)$$

where n_ω and $n_{2\omega}$ are the refractive indices as seen by the fundamental and second-harmonic waves, respectively. The molecular hyperpolarizability is given by [15]

$$\langle \beta \rangle = \beta_\perp \langle \cos^3\psi \rangle \qquad (13)$$

which, when using equations (6) and (4) with $\cos^3\psi$ in the integrand instead of $\cos\psi$, gives the *same* functional dependence of $\langle \beta \rangle$ on the mole fraction x_A of chiral species A as that of $\langle \mu \rangle$ in equation (8):

$$\langle \beta \rangle = \beta_\perp \frac{\kappa' x_A}{1 + \gamma x_A^2}, \qquad (14)$$

where the only difference is the parameter κ', which is slightly different from κ and given by

$$\kappa' = \frac{\dfrac{1{\cdot}5kT}{a_2\theta} + \theta}{\dfrac{4k^2T^2}{a_1 a_2 \theta^2} + \dfrac{a_2}{a_1}\theta^2}. \qquad (15)$$

The parameter γ, however, is the same as in equation (9). The second-order non-linear optical susceptibility is then obtained as

$$\chi^{(2)} = NF\langle \beta \rangle = F \frac{\beta_\perp \kappa'}{b_A} \eta \frac{x_A^2}{[1 + \gamma x_A^2][1 + (\eta - 1)x_A]}. \qquad (16)$$

Equations (10) and (16) imply that if the spontaneous polarizations and the second-order non-linear optical susceptibilities at two different mole fractions $x_A = x_1, x_2$

are compared, the respective relationships should be equal, i.e.

$$\frac{P_S(x_2)}{P_S(x_1)} = \frac{\chi^{(2)}(x_2)}{\chi^{(2)}(x_1)}. \tag{17}$$

From the measurements of the spontaneous polarization in figure 7, the susceptibility for **A2c** is expected to be about 8 times greater than that for the mixture **A1**:**A2** 30:70 and about 6·4 times greater than that for the mixture **A1**:**A2** 35:65.

7. Second-harmonic generation in the QBS geometry

Second-harmonic generation in ferroelectric liquid crystals is usually measured in the homeotropic geometry in thick (10–200 μm) cells, with the electric field applied in the plane of the glass plates instead of across it. In our case, however, second-harmonic generation was measured in thin (2–4 μm) planar aligned samples in the quasi-bookshelf (QBS) geometry, where the smectic layers are essentially perpendicular to the glass plates.

The sample geometry is shown in figure 8. The y-axis is chosen to be normal to the glass plates, which corresponds to it being parallel to the polar C_2-axis of a sample with bookshelf geometry. The z-axis is chosen parallel to the optic axis, i.e. the director. The x-axis thus lies in the plane of the cell glass plates, in a direction perpendicular to the director. The angles ϑ and φ denote the angle of incidence and the azimuthal angle, respectively, and are measured with respect to the y and z axes, respectively. The angle ϑ denotes the incidence angle in the material. The incidence angle outside the sample is greater, as the light is refracted at the air–glass interface. This angle will in the following text be denoted α. The refractive indices of the glass and the material

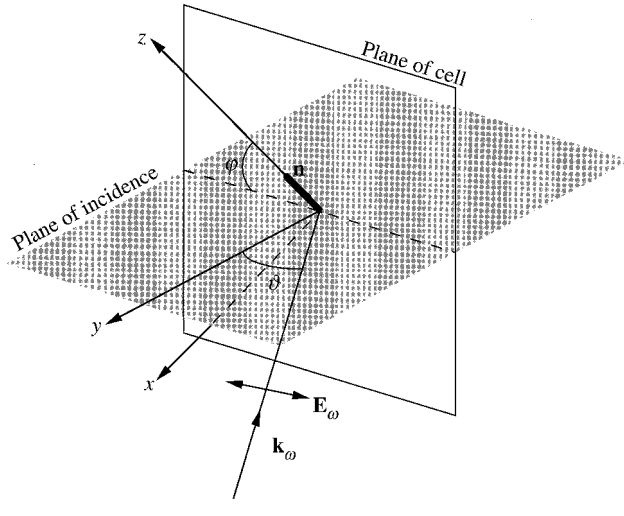

Figure 8. The geometry and the definition of the coordinate system for the SHG measurements.

are similar, so the refraction at the glass–material interface has been neglected. The angles of incidence ϑ and α are then related by Snell's law as

$$\sin\alpha = n_g \sin\vartheta \tag{18}$$

where $n_g = 1{\cdot}52$ is the refractive index of glass. When $\varphi = 0$ the plane of incidence coincides with the yz-plane, and so the optic axis lies in the plane of incidence. When $\varphi = 90°$ the plane of incidence instead coincides with the xy-plane, and the optic axis is perpendicular to the plane of incidence. With both the fundamental and second-harmonic waves polarized in the plane of incidence (pp-polarizations), $\varphi = 0$ corresponds to both of them being extraordinary waves (eee-interaction), and $\varphi = 90°$ corresponds to both of them being ordinary waves (ooo-interaction). Similarly, ps-polarizations (second-harmonic wave polarized perpendicular to the plane of incidence) correspond to the eeo-interaction when $\varphi = 0$, and to the ooe-interaction when $\varphi = 90°$.

The SHG conversion efficiency e_{SHG} is given by [1]

$$e_{SHG} = \frac{I_{2\omega}}{I_\omega} = \frac{2}{\varepsilon_0^3 c_0^3}\frac{d_{eff}^2 \omega^2 l^2}{n_\omega^2 n_{2\omega}} I_\omega \operatorname{sinc}^2\left(\frac{\Delta k l}{2\pi}\right) \tag{19}$$

where I_ω and $I_{2\omega}$ are the intensities of the fundamental and second-harmonic beams, respectively, d_{eff} is the effective second-order NLO coefficient ($2d = \chi^{(2)}$), ω is the (angular) frequency of the fundamental light, l is the interaction length, and n_ω and $n_{2\omega}$ are the refractive indices as seen by the fundamental and second-harmonic beams, respectively. The factor $\operatorname{sinc}^2 x \equiv \sin^2(\pi x)/(\pi x)^2$ takes into account the phase mismatch $\Delta k = k_{2\omega} - 2k_\omega = 4\pi(n_{2\omega} - n_\omega)/\lambda_0$. The quantities d_{eff} and l depend on the angle of incidence, ϑ. If any of the waves is extraordinary, then n_ω, $n_{2\omega}$ and Δk also depend on ϑ. The interaction length is given by

$$l(\vartheta) = \frac{l_0}{\cos\vartheta} \tag{20}$$

where l_0 is the cell thickness. The refractive index for an extraordinary wave with a wavevector making an angle ζ with the director or optic axis is given by

$$\frac{1}{n_e^2(\zeta)} = \frac{\cos^2\zeta}{n_o^2} + \frac{\sin^2\zeta}{n_e^2}. \tag{21}$$

For the case $\varphi = 90°$ the director is perpendicular to the plane of incidence, whence the wave-vector is perpendicular to the director for all angles of incidence, ϑ. Hence, $\zeta = \pi/2$ independently of ϑ. For the case $\varphi = 0$, however, the director is in the plane of incidence and ζ is related to the angle of incidence ϑ as $\zeta = \pi/2 - \vartheta$. Rewriting equation (21) for the case $\varphi = 0$ in terms of ϑ,

we thus get

$$\frac{1}{[n_e^{\omega}(\vartheta)]^2} = \frac{\sin^2\vartheta}{(n_o^{\omega})^2} + \frac{\cos^2\vartheta}{(n_e^{\omega})^2}$$

and

$$\frac{1}{[n_e^{2\omega}(\vartheta)]^2} = \frac{\sin^2\vartheta}{(n_o^{2\omega})^2} + \frac{\cos^2\vartheta}{(n_e^{2\omega})^2}. \tag{22}$$

The expression for d_{eff} for collinear second-harmonic generation is formally given by

$$d_{\text{eff}} = \hat{e}_{2\omega}\mathbf{d} : \hat{e}_{\omega}\hat{e}_{\omega} \tag{23}$$

where the $\hat{e}_{\omega}$ and $\hat{e}_{2\omega}$ are unit vectors describing the direction of the linearly polarized fundamental and second-harmonic waves, respectively, and where **d** is the tensor of the non-linear optical coefficients. In the case of C_2 point group symmetry, which applies to ferroelectric liquid crystals and pyroelectric liquid crystal polymers, the **d**-tensor is given by

$$\mathbf{d} = \begin{pmatrix} 0 & 0 & 0 & d_{14} & 0 & d_{16} \\ d_{16} & d_{22} & d_{23} & 0 & d_{14} & 0 \\ 0 & 0 & 0 & d_{23} & 0 & d_{14} \end{pmatrix} \tag{24}$$

where the polar C_2 axis (the spontaneous polarization) is parallel to the y-axis, and where Kleinman symmetry has been assumed (i.e. the non-linearity is completely non-resonant). From equations (23) and (24) the expressions for d_{eff} for the cases $\varphi = 0$ and $\varphi = 90°$ with pp- and ps-polarizations, respectively, can be found for the planar FLC/PLCP cell geometry to be:

$$\begin{aligned}
&d_{\text{eff}}(\vartheta) = 3d_{16}\cos^2\vartheta\sin\vartheta + d_{22}\sin^3\vartheta && \varphi = 90° \text{ pp (ooo)}\\
&d_{\text{eff}}(\vartheta) = -d_{14}\sin 2\vartheta && \varphi = 90° \text{ ps (ooe)}\\
&d_{\text{eff}}(\vartheta) = 3d_{23}\cos^2\vartheta\sin\vartheta + d_{22}\sin^3\vartheta && \varphi = 0° \text{ pp (eee)}\\
&d_{\text{eff}}(\vartheta) = d_{14}\sin 2\vartheta && \varphi = 0° \text{ ps (eeo)}
\end{aligned} \tag{25}$$

where the refraction at the glass–liquid crystal interface has been neglected. Equations (25) are valid under phase-matching conditions, where all the interacting waves are collinear (equivalent to $\Delta k = 0$). With a phase mismatch, the interacting waves have slightly different directions, as given by Δk [1]. In thin samples, however, the deviation from collinearity should still be small as the interaction length is short, whence equations (25) are taken to be valid in the subsequent analysis with this approximation.

8. SHG experiments and analysis

A very clear and easily detectable SH signal from sample **A** is shown in figure 9(*a*) as a function of the angle of incidence at $\varphi = 180°$. The signal shows a good symmetry profile. Next, the SH signal at $\varphi = 90°$ for pp-polarizations is shown in figure 9(*b*). In this case, the minimum of the symmetry profile is shifted about 13° towards positive α. Figures 9(*a*) and 9(*b*) thus suggest that the polar C_2-axis of this sample makes an angle of about 13° in terms of α with the y-axis, and that it lies

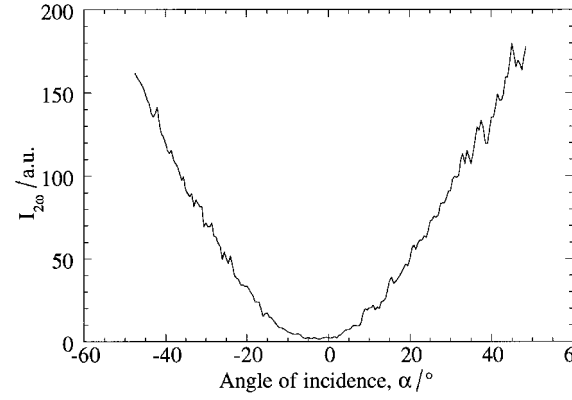

(*a*)

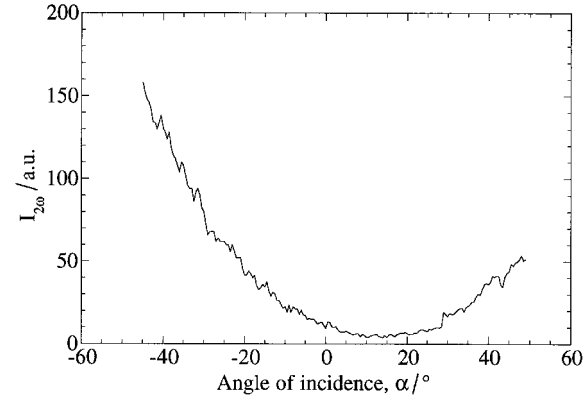

(*b*)

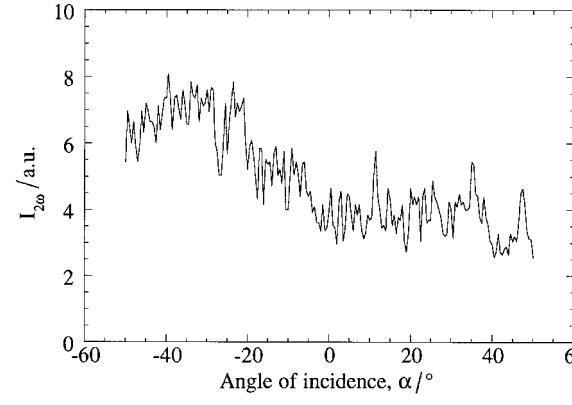

(*c*)

Figure 9. The SH signal (532 nm) from sample **A** as a function of angle of incidence. (*a*) $\varphi = 180°$, pp-polarizations, eee-interaction; (*b*) $\varphi = 90°$, pp-polarizations, ooo-interaction; (*c*) $\varphi = 180°$, ps-polarizations, eeo-interaction.

in the xy-plane. Finally, the SH signal at $\varphi = 90°$ for ps-polarizations is shown in figure 9 (c), and is found to be about one order of magnitude weaker than for pp-polarizations.

The dependence of the SH signal on the azimuthal angle φ was measured for sample **A**, and is shown in figure 10 for the case $\alpha = -42{\cdot}0°$. Four lobes of maximum SH intensity were found. If the sample is turned around the y-axis through 180°, the same SH intensity is expected to be found, since in the planar bookshelf geometry both the optic axis and the polar axis are invariant to such a rotation. In this case, however, since the polar axis is tilted with respect to the y-axis, a 180° rotation around the y-axis will also rotate the tilt plane of the polar axis by 180°. Then, the angle between the polarization vector of the fundamental light and the spontaneous polarization of the sample will be different upon such a rotation, and the SH signal intensity will be different as well. This is clearly seen in figure 10 by the fact that the lobes around 90° and 270° have a very different magnitude. That the tilt plane of the polar axis of the sample is the xy-plane is also evident in figure 10 from the similar magnitudes of the lobes around 0° and 180°, in which situation the xy-plane is perpendicular to the plane of incidence.

According to equation (19) the intensity of the SH light is proportional to the square of the fundamental light intensity

$$I_{2\omega} \propto I_{\omega}^{2}. \tag{26}$$

The SH intensity was therefore measured as a function of fundamental light intensity for the case $\alpha = -42{\cdot}0°$, $\varphi = 90°$, and the result is shown in figure 11. Equation (26) is obeyed by the SH signal of the polymer, confirming the true electronic origin of the second harmonic generation in the polymer.

A measurement on a reference sample of a 500 μm thick slab of $LiNbO_3$ was performed for the same set-up that was used for the measurements on Sample **A**, under the same circumstances and at the same intensity of fundamental light; this is shown in figure 12. The SH intensity units in figures 9 (a)–12 are thus directly comparable. The $LiNbO_3$ crystal was rotated around its polar z-axis. The intensity at normal incidence thus corresponded to the coefficient d_{33} as being responsible for the SHG, but being non-phase matched.

In order to analyse the measurements and estimate the non-linear optical coefficients of the polymer **A2c**, it is convenient to rewrite equations (19), (20) and (25) as a product of a dimensionless factor $i(\vartheta)$ including all of the angular dependence of the SH signal and a constant factor K containing the dimension. This means that K will contain one of the independent elements of the **d**-tensor, which in the case of C_2 symmetry is

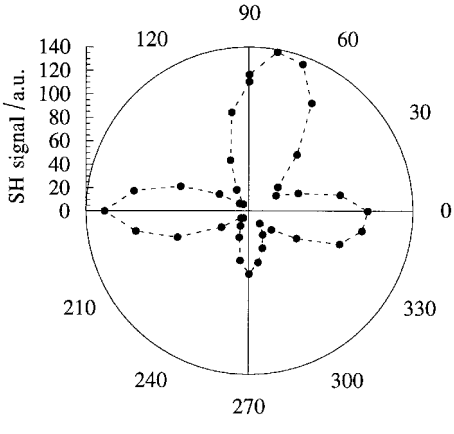

Figure 10. The SH signal (532 nm) from sample **A** as a function of azimuthal angle, at $\alpha = -42{\cdot}0°$. Polarization combination: pp.

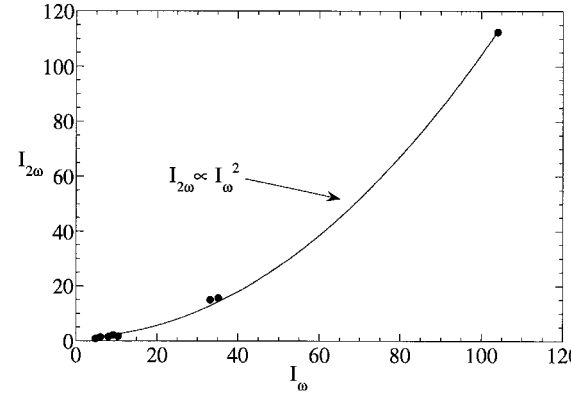

Figure 11. The SH signal $I_{2\omega}$ (532 nm) from sample **A** as a function of fundamental light intensity, I_{ω}, at $\alpha = -42{\cdot}0°$. Polarization combination: pp. The solid line is a square function.

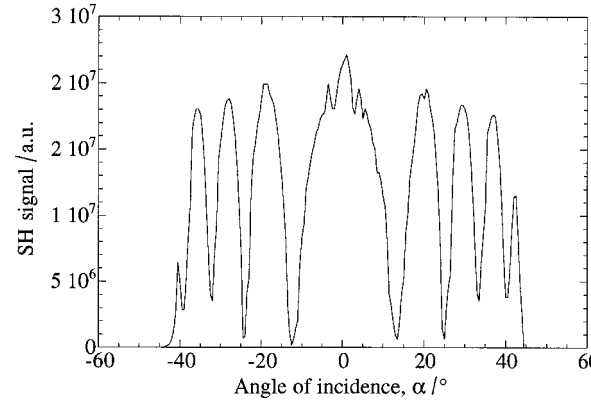

Figure 12. The SH signal $I_{2\omega}$ (532 nm) from a 500 μm thick slab of $LiNbO_3$, used as reference for the evaluation of the SH signal from sample **A**, as a function of incidence angle, α. The polarization combination is ss, being equivalent to the eee-interaction—hence, the signal is non-phase matched. At normal incidence, $\alpha = 0$, $d_{\text{eff}} = d_{33}$.

most conveniently chosen to be d_{22}. We thus have the following relations and definitions:

$$I_{2\omega}(\vartheta) = K\, i(\vartheta) \tag{27}$$

where

$$K = \frac{8\pi^2 d_{22}^2 I_\omega^2}{\varepsilon_0^3 c_0} \tag{28}$$

and where

$$i(\vartheta) = \frac{\delta_{\text{eff}}^2(\vartheta)}{n_\omega^2(\vartheta) n_{2\omega}(\vartheta)} \frac{\xi_0^2}{\cos^2\vartheta} \frac{\sin^2\sigma(\vartheta)}{\sigma^2(\vartheta)}. \tag{29}$$

The symbols σ and ξ_0 are defined as

$$\sigma(\vartheta) = 2\pi \frac{\xi_0}{\cos\vartheta} |n_{2\omega}(\vartheta) - n_\omega(\vartheta)| \tag{30}$$

and

$$\xi_0 \equiv \frac{l_0}{\lambda_0}. \tag{31}$$

The reduced effective non-linear optical coefficient $\delta_{\text{eff}}(\vartheta)$ is given by

$$\begin{aligned}
&\delta_{\text{eff}}(\vartheta) = 3\delta_{16}\cos^2\vartheta\sin\vartheta + \sin^3\vartheta \quad \text{(ooo)} \quad \text{(a)}\\
&\delta_{\text{eff}}(\vartheta) = -\delta_{14}\sin 2\vartheta \quad \text{(ooe)} \quad \text{(b)}\\
&\delta_{\text{eff}}(\vartheta) = 3\delta_{23}\cos^2\vartheta\sin\vartheta + \sin^3\vartheta \quad \text{(eee)} \quad \text{(c)}\\
&\delta_{\text{eff}}(\vartheta) = \delta_{14}\sin 2\vartheta \quad \text{(eeo)} \quad \text{(d)}
\end{aligned} \tag{32}$$

where

$$\delta_{\text{eff}}(\vartheta) \equiv \frac{d_{\text{eff}}(\vartheta)}{d_{22}} \Rightarrow \delta_{16} \equiv \frac{d_{16}}{d_{22}}, \qquad \delta_{23} \equiv \frac{d_{23}}{d_{22}}, \qquad \delta_{14} \equiv \frac{d_{14}}{d_{22}}. \tag{33}$$

In figures 13(*a*) and 13(*b*) are shown curve fits to equation (27), with equations (22) and (28)–(33) inserted into it. The internal angle of incidence was first calculated by equation (18). Since the C_2-axis was inclined with respect to the y-axis, the minimum position of the curves was then shifted in order to coincide with zero angle of incidence, so that the angle ϑ given in the figures is the internal angle of incidence with respect to the polar C_2-axis, enabling equation (27) to be fitted correctly to the data. In the fits, it is necessary to give the ordinary and extraordinary refractive indices at the two wavelengths—these cannot be found from the fits since the sample is too thin to be able to show several Maker Fringes. Based upon a refractive index measurement for the isotropic phase with the m-line method yielding $n_{\text{iso}} = 1{\cdot}556$ for **A2c**, and a birefringence in the visible $n_e^{2\omega} - n_o^{2\omega}$ of about 0·1 [22], together with an assumed dispersion of 0·05 typical of FLCs, the following values

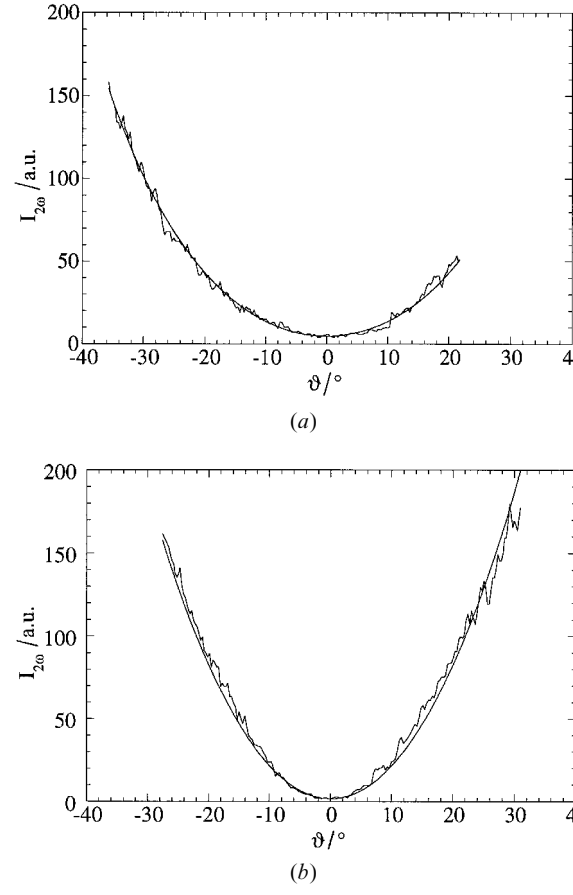

Figure 13. A curve fit of equation (27) to the SH signal from sample **A** as a function of internal angle of incidence, ϑ, for (*a*) $\varphi = 90°$, ooo-interaction and (*b*) $\varphi = 180°$, eee-interaction.

of the refractive indices have been used in the fits:

$$n_e^{\omega} = 1{\cdot}57 \qquad n_o^{\omega} = 1{\cdot}47 \qquad n_e^{2\omega} = 1{\cdot}62 \qquad n_o^{2\omega} = 1{\cdot}52. \tag{34}$$

With $\xi_0 = 2$ the fits in figures 13(*a*) and 13(*b*) yielded the following values for the parameters:

$$\begin{aligned}
K &= (339 \pm 13)\ \text{a.u.}\\
\delta_{16} &= 0{\cdot}296 \pm 0{\cdot}008\\
\delta_{23} &= 0{\cdot}496 \pm 0{\cdot}002.
\end{aligned} \tag{35}$$

The sensitivity of the fit parameters to variations of the refractive indices was checked as well. A variation of about 8% of the refractive indices gave variations of about 17% in K and 21% in the δ values. We thus get the following ranges for the values of the fit parameters:

$$\begin{aligned}
K &= (339 \pm 13 \pm 58)\ \text{a.u.}\\
\delta_{16} &= 0{\cdot}296 \pm 0{\cdot}008 \pm 0{\cdot}063\\
\delta_{23} &= 0{\cdot}496 \pm 0{\cdot}002 \pm 0{\cdot}104.
\end{aligned} \tag{36}$$

According to equation (27) the SH signal from the polymer (P) can be compared with that of $LiNbO_3$ (L) in the following way:

$$\left.\begin{aligned} I^{P}_{2\omega}(\vartheta_P) &= K_P i_P(\vartheta_P) \\ I^{L}_{2\omega}(\vartheta_L) &= K_L i_L(\vartheta_L) \end{aligned}\right\} \Rightarrow K_P = \frac{I^{P}_{2\omega}(\vartheta_P)}{I^{L}_{2\omega}(\vartheta_L)} \frac{i_L(\vartheta_L)}{i_P(\vartheta_P)} K_L \tag{37}$$

where the SH signals are compared at incidence angles ϑ_P and ϑ_L, not necessarily being equal. For the case $\vartheta_L = 0°$ (normal incidence) the effective d-coefficient of $LiNbO_3$ is d_{33}, i.e. $\delta^{P}_{eff}(0) = 1$. The refractive indices of $LiNbO_3$ are

$$n_e^{\omega} = 2{\cdot}25 \qquad n_o^{\omega} = 2{\cdot}16 \qquad n_e^{2\omega} = 2{\cdot}34 \qquad n_o^{2\omega} = 2{\cdot}24. \tag{38}$$

Normal incidence implies (eee)-interaction. With $\xi_0 = 500/1{\cdot}016 = 492$ this gives $i_L(0) = 0{\cdot}2547131$. The intensity at normal incidence (see figure 12) was $I^{L}_{2\omega}(0) = 2{\cdot}4 \times 10^7$ a.u. Equation (37) may in this case be rewritten as

$$d^{P}_{22} = \left(K_P \frac{i_L(0)}{I^{L}_{2\omega}(0)} \right)^{1/2} d^{L}_{33} \tag{39}$$

which with the above values gives $d_{22} = (0{\cdot}083 \pm 0{\cdot}002 \pm 0{\cdot}007)$ pm V^{-1} for the polymer **A2c**. With equation (36), we thus get the following values for the d-coefficients:

$$d_{22} = (0{\cdot}083 \pm 0{\cdot}007) \text{ pm V}^{-1}$$
$$d_{16} = (0{\cdot}025 \pm 0{\cdot}008) \text{ pm V}^{-1}$$
$$d_{23} = (0{\cdot}041 \pm 0{\cdot}013) \text{ pm V}^{-1}$$

where the error limits are due almost entirely to the uncertainty of the refractive indices of **A2c**.

In the measurement of figure 9(*c*) the coefficient d_{14} gives rise to the second-harmonic generation. The signal was about 20 times weaker than that in figure 9(*b*), giving

$$d_{14} \sim 0{\cdot}01 - 0{\cdot}02 \text{ pm V}^{-1}.$$

The SH signal obtained for sample **B** is shown in figure 14 as a function of angle of incidence. The signal profile is symmetric. As a rough check of the results on sample **A** a comparison of this signal with a poled polymer of PMMA-DR1 of a similar thickness gave the SH signal intensity $I_{2\omega}$ of the polymer **A2c** as roughly two orders of magnitude lower than that of the PMMA-DR1 polymer. This implies that the second-order non-linear optical coefficient of **A2c** is about one order of magnitude lower than that of PMMA-DR1. For PMMA-DR1 $d_{33} = 2{\cdot}5$ pm V^{-1} [1], giving the estimation of $d_{A2c} \sim 0{\cdot}2$ pm V^{-1} for **A2c** which is of the same order of magnitude as $d_{22} \sim 0{\cdot}1$ pm V^{-1} according to the analysis above.

Measurements of second-harmonic generation on sample **D** with the *monomer* **A2c** were also carried out for several combinations of ϑ and φ, under the application of a d.c. bias voltage of 100 V. An example is shown in figure 15. The SH signal was easily detectable, and of a similar or greater strength as that for the crosslinked samples. A more detailed analysis of these measurements will be presented elsewhere.

Second-harmonic generation was previously demonstrated by us in [20] for both crosslinked and monomeric samples of mixtures of **A1** and **A2** in the molar proportions 30:70 and 35:65, respectively. The SH signal from the **A1**:**A2** mixtures was much weaker and more difficult to detect than that from **A2c**, in accordance with the expectations from equation (17). The upper limit for the d-coefficient of the 35:65 **A1**:**A2** mixture

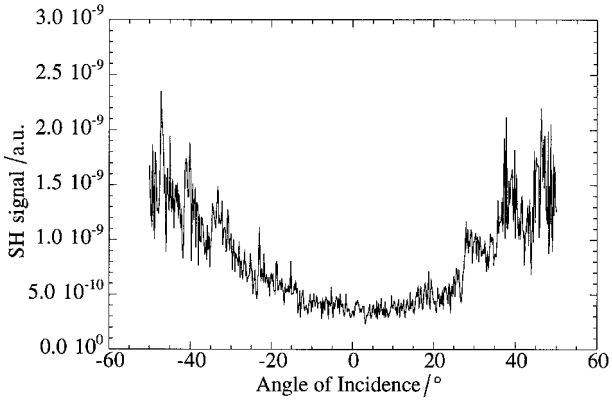

Figure 14. The SH signal (550 nm) from sample **B** as a function of angle of incidence. The signal is two orders of magnitude weaker than that from a film of the poled polymer PMMA-DR1 of a similar thickness.

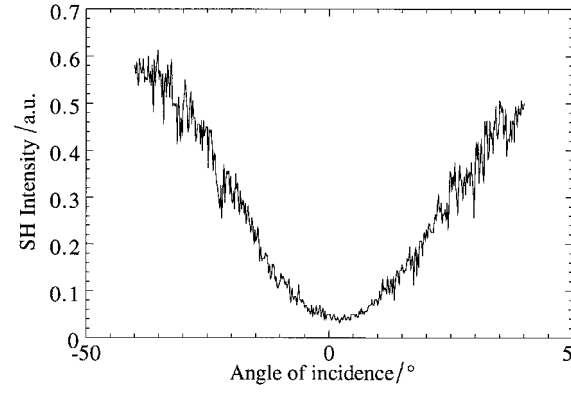

Figure 15. The SH signal (550 nm) from the monomer **A2c**, sample **D**, as a function of angle of incidence, at $\varphi = 195°$. Polarization combination: pp. A d.c. bias voltage of 100 V over 4 μm is applied.

is 0·017 pm V^{-1}†, which gives $d_{22,\mathbf{A2c}}/d_{\mathbf{A1:A2}} > 4{\cdot}9$. This is consistent with the spontaneous polarization data, giving $P_{S,\mathbf{A2c}}/P_{S,\mathbf{A1:A2}} = 160/25 = 6{\cdot}4$ for the 35:65 **A1**:**A2** mixture.

9. Discussion

The SHG measurements on the polymer **A2c** very clearly confirm the presence of a permanent, thermally stable polar order. The thermal stability of the material was checked by another measurement on sample **B** about one month after the first measurement in figure 14 was performed. A clear SH signal was still obtained, albeit about half as strong as the signal shown in figure 14. In contrast, no SH signal whatsoever could be detected for the PMMA-DR1 poled polymer one month after the first measurement. In comparison with conventional poled polymers, the pyroelectric liquid crystal polymer has a very good thermal stability.

The shift of the minimum of the SH signal in figure 9 (*b*) by about 13°, implying that the spontaneous polarization vector is tilted with respect to the normal of the cell glass plates, seems to be characteristic of crosslinked **A2c**. Subsequent measurements of second-harmonic generation in polymerized samples of **A1b** and **A2c** (without any electric field applied) have shown this effect only for **A2c** and not for **A1b**. These results will be published elsewhere.

The method of analysis presented in this work is suitable for the planar FLC geometry (SSFLC or QBS). Usually, the homeotropic geometry is used for SHG measurements. In our case, however, **A2c** is a very tightly twisted SmC* material, requiring a threshold electric field of 3 V μm^{-1} in order to unwind the helix (for most FLCs, only a threshold of the order of 0·1 V μm^{-1} is required). This fact has made it impossible so far to be able to unwind the helix in the homeotropic geometry and to keep it unwound during the polymerization. Independently of this, however, it is useful in itself to be able to make an analysis of planar oriented samples, since this is the most probable geometry for any non-linear optical FLC/PLCP device applications, such as non-linear optical waveguides [10, 20].

The estimated value of the d coefficient of **A2c** of the order of 0·08 pm V^{-1} is almost one order of magnitude lower than that reported for compound **I**, having a similar chemical structure [7]. The spontaneous polarization of compound **I**, however, was reported to be about 500 nC cm^{-2}, indicating that the non-linear optical coefficient of **I** should be expected to be higher than that of **A2c**.

In order to ameliorate the NLO activity of the PLCPs further, antiferroelectric structures may be considered. Another possibility would be to make structures like **II** crosslinkable. Further synthetic work in these directions is currently under way.

10. Conclusions

(1) We have demonstrated clear second-harmonic generation in crosslinked, polymeric samples as well as in a monomeric sample of the bifunctional, chiral compound **A2c**.

(2) The second-order non-linear optical coefficients of **A2c** are almost one order of magnitude larger than for crosslinked mixtures of **A1** and **A2** with a 30–35 mol % chiral content.

(3) Increasing the chiral strength increases both the spontaneous polarization and the second-order non-linear optical coefficients.

(4) The non-linear dependence of the spontaneous polarization on the mole fraction of chiral monomers could be well accounted for in terms of the different molecular sizes of the components of the mixture, as well as of a microscopic model for the biased rotational distribution of lateral dipole moments about the molecular long axis.

(5) The high temperature phase of the monomer **A2c** is *not* a SmA* phase. It is most likely a very tightly twisted cholesteric phase.

(6) The thermal stability of the polar order in the crosslinked polymer is very good, in comparison with the conventionally poled polymer PMMA-DR1.

(7) There is some residual molecular motion in the crosslinked polymer networks, although it is very small—the angular deviation from the locked-in tilt angle of the network is of the order of 0·1°–0·4°.

† The SH signal for a 2 μm sample of a 35:65 mol % **A1**:**A2** mixture was reported in reference [20] to be about 1000 times smaller than the signal from a quartz reference. In order to compare the signals, that of the sample cell should be extrapolated to the signal that would be obtained from a sample where the interaction length l is half the coherence length $l_C = 2\pi/\Delta k$ of the interaction. The extrapolated signal would thus be a factor of

$$\sin^2\left(\pi\frac{l_C/2}{l_C}\right)\Big/\sin^2\left(\pi\frac{l}{l_C}\right)\approx 1/(\pi l/l_C)^2 = \pi^{-2}l_C^2/l^2$$

greater by way of equation (29) with $\sigma = \Delta k l/2 = \pi l/l_C$. Typical coherence lengths are about 10 μm, and since $l > l_0 = 2\,\mu m$, the extrapolated SH signal of the sample would be a factor of $< \pi^{-2}(10/2)^2 = (5/\pi)^2$ greater. This gives the relation between the d-coefficients of **A1**:**A2** and quartz as $d^2_{\mathbf{A1:A2}} < [(5/\pi)^2/1000]\,d^2_{\mathrm{Quartz}}$, which for $d_{\mathrm{Quartz}} = 0{\cdot}34$ pm V^{-1} gives $d_{\mathbf{A1:A2}} < 0{\cdot}017$ pm V^{-1}. The reported higher value of about 0·4 pm V^{-1} in reference [20] for the **A1**:**A2** mixtures was due to an overestimated coherence length.

(8) At frequencies in the sub-MHz range of an applied electric field, there is a spontaneous production of heat from the polymer network, corresponding to a resonance of the network.

Financial support from the National Foundation for Strategic Research of Sweden is gratefully acknowledged. Prof. K. Yoshino, Asst. Prof. M. Ozaki and Dr S. Uto of the University of Osaka, Japan are gratefully acknowledged for their hospitality during a short visit of DSH, when the SHG measurements on sample **A** were performed. Dr J. Lindström of the National Defence Research Establishment, S-172 90 Stockholm, Sweden is gratefully acknowledged for providing the poled polymer PMMA-DR1. Dr F. Giesselmann of the Technical University of Clausthal, Germany, is gratefully acknowledged for discussions of the cholesteric-like phase of the monomer **A2c**.

Appendix: The non-linear dependence of the volume fraction on the mole fraction

In a binary mixture consisting of two components A and B the mole fractions $x_{A,B}$ and volume fractions $v_{A,B}$ are defined as

$$x_A = \frac{X_A}{X_A + X_B} \qquad x_B = \frac{X_B}{X_A + X_B} \qquad x_A + x_B = 1 \tag{A1}$$

$$v_A = \frac{V_A}{V_A + V_B} \qquad v_B = \frac{V_B}{V_A + V_B} \qquad v_A + v_B = 1 \tag{A2}$$

where $X_{A,B}$ and $V_{A,B}$ are the numbers and macroscopic volumes of the components A and B, respectively. The microscopic volumes $b_{A,B}$ of an A and a B molecule, respectively, are given by the defining relations

$$V_A = b_A X_A \qquad V_B = b_B X_B. \tag{A3}$$

Finally, we define the parameter η as the ratio between the volumes of an A and a B molecule:

$$\eta \equiv \frac{b_A}{b_B}. \tag{A4}$$

From Equations (A3) and (A4) we get

$$\frac{V_A}{V_B} = \frac{b_A X_A}{b_B X_B} = \eta \frac{X_A}{X_B} \tag{A5}$$

which, with equation (A1) and (A2), gives

$$\frac{v_A}{v_B} = \eta \frac{x_A}{x_B} \qquad \text{or} \qquad \frac{v_A}{1 - v_A} = \eta \frac{x_A}{1 - x_A}. \tag{A6}$$

A rewriting of the second version of equation (A6) now gives directly equation (2) in the text:

$$v_A = \frac{\eta x_A}{1 + (\eta - 1) x_A}. \tag{2}$$

The number density N of chiral molecules A in the mixture is the volume fraction of A divided by the molecular volume of A, according to the following:

$$\begin{aligned} N &= \frac{X_A}{V_{tot}} = \frac{X_A \dfrac{X_A + X_B}{X_A + X_B}}{V_A + V_B} = x_A \frac{X_A + X_B}{b_A X_A + b_B X_B} \\ &= \frac{x_A}{b_A \left(x_A + \dfrac{1}{\eta} x_B \right)} = \frac{1}{b_A} \frac{x_A}{\dfrac{1}{\eta} [\eta x_A + (1 - x_A)]} \\ &= \frac{1}{b_A} \frac{\eta x_A}{1 + (\eta - 1) x_A} = \frac{1}{b_A} v_A. \end{aligned} \tag{A7}$$

References

[1] Prasad, P. N., and Williams, D. J., 1991, *Introduction to Nonlinear Optical Effects in Molecules and Polymers*, 1st edn (New York: John Wiley).

[2] Meyer, R. B., Liébert, L., Strzelecki, L., and Keller, P., 1975, *J. Physique Lett.*, **36,** L69.

[3] Clark, N. A., and Lagerwall, S. T., 1980, *Appl. Phys. Lett.*, **36,** 899.

[4] Vtyurin, A. N., Yermakov, V. P., Ostrovsky, B. I., and Shabanov, V. F., 1981, *Krystallografiya*, **26,** 546.

[5] Shtykov, N. M., Barnik, M. I., Beresnev, L. A., and Blinov, L. M., 1985, *Mol. Cryst. liq. Cryst.*, **124,** 379.

[6] Walba, D. M., Ros, M. B., Clark, N. A., Shao, R., Johnson, K. M., Robinson, M. G., Liu, J. Y., and Doroski, D., 1991, *Mol. Cryst. liq. Cryst.*, **198,** 51.

[7] Liu, J.-Y., Robinson, M. G., Johnson, K. M., Walba, D. M., Ros, M. B., Clark, N. A., Shao, R., and Doroski, D., 1991, *J. appl. Phys.*, **70,** 3426.

[8] Schmitt, K., Herr, R.-P., Schadt, M., Fünfschilling, J., Buchecker, R., Chen, X. H., and Benecke, C., 1993, *Liq. Cryst.*, **14,** 1735.

[9] Taguchi, A., Ouchi, Y., Takezoe, H., and Fukuda, A., 1989, *Jpn. J. appl. Phys.*, **28,** L997.

[10] Liu, J. Y., Robinson, M. G., Johnson, K. M., and Doroski, D., 1990, *Optics Lett.*, **15,** 267.

[11] Ozaki, M., Utsumi, M., Gotou, T., Morita, Y., Daido, K., Sadohara, Y., and Yoshino, K., 1991, *Ferroelectrics*, **121,** 259.

[12] Kajikawa, K., Isozaki, T., Takezoe, H., and Fukuda, A., 1992, *Jpn. J. appl. Phys.*, **31,** L679.

[13] Ozaki, M., Utsumi, M., Uchiyama, Y., and Yoshino, K., 1993, *Ferroelectrics*, **148,** 337.

[14] Park, B., Lim, M., Lee, J.-H., Kim, J.-H., and Lee, S.-D., 1996, *Ferroelectrics*, **179,** 231.

[15] Stanley, M., Day, S. E., Dunmur, D. A., and Grayson, M., 1996, *Ferroelectrics*, **179,** 249.

[16] Ozaki, M., Utsumi, M., Yoshino, K., and Skarp, K., 1993, *Jpn. J. appl. Phys.*, **32,** L852.

[17] Wischerhoff, E., Zentel, R., Redmond, M., Mondain-Monval, O., and Coles, H., 1994, *Macromol. Chem. Phys.*, **195,** 1593.

[18] Kobayashi, K., Watanabe, T., Uto, S., Ozaki, M., Yoshino, K., Svensson, M., Helgee, B., and Skarp, K., 1996, *Jpn. J. appl. Phys.*, **35,** L104.
[19] Trollsås, M., Sahlén, F., Gedde, U. W., Hult, A., Hermann, D., Rudquist, P., Komitov, L., Lagerwall, S. T., Stebler, B., Lindström, J., and Rydlund, O., 1996, *Macromolecules*, **29,** 2590.
[20] Hult, A., Sahlén, F., Trollsås, M., Lagerwall, S. T., Hermann, D., Komitov, L., Rudquist, P., and Stebler, B., 1996, *Liq. Cryst.*, **20,** 23.
[21] Sahlén, F., Trollsås, M., Hult, A., Gedde, U. W., Hermann, D., Rudquist, P., Komitov, L., and Lagerwall, S. T., 1998, *Liq. Cryst.* (submitted).
[22] Trollsås, M., Orrenius, C., Sahlén, F., Gedde, U. W., Norin, T., Hult, A., Hermann, D., Rudquist, P., Komitov, L., Lagerwall, S. T., and Lindström, J., 1996, *J. Am. chem. Soc.*, **118,** 8542.
[23] Patel, J. S., and Meyer, R. B., 1987, *Phys. Rev. Lett.*, **58,** 1538.
[24] Rudquist, P., Komitov, L., and Lagerwall, S. T., 1994, *Phys. Rev. E*, **50,** 4735.
[25] Garoff, S., and Meyer, R. B., 1977, *Phys. Rev. Lett.*, **38,** 848.
[26] Zeks, B., Carlsson, T., Filipic, C., and Urbanc, B., 1988, *Ferroelectrics*, **84,** 3.
[27] Urbanc, B., and Zeks, B., 1989, *Liq. Cryst.*, **5,** 1075.